Optimized efficiency in InP nanowire solar cells with accurate 1D analysis

Chen, Yang; Kivisaari, Pyry; Pistol, Mats Erik; Anttu, Nicklas

Published in:
Nanotechnology

DOI:
10.1088/1361-6528/aa9e73

2018

Optimized efficiency in InP nanowire solar cells with accurate 1D analysis

Yang Chen[1,*], *Pyry Kivisaari*[1], *Mats-Erik Pistol*[1] *and Nicklas Anttu*[1,2,*]

1. Division of Solid State Physics and NanoLund, Lund University, Box 118, 22100 Lund, Sweden
2. Sol Voltaics AB, Scheelevägen 22, SE-22363 Lund, Sweden

*Email: yang.chen@ftf.lth.se, nicklas.anttu@ftf.lth.se

Abstract

Semiconductor nanowire arrays are a promising candidate for next generation solar cells due to enhanced absorption and reduced material consumption. However, to optimize their performance, time consuming three-dimensional (3D) opto-electronics modeling is usually performed. Here, we develop an accurate one-dimensional (1D) modeling method for the analysis. The 1D modeling is about 400 times faster than 3D modeling and allows direct application of concepts from planar pn-junctions on the analysis of nanowire solar cells. We show that the superposition principle can break down in InP nanowires due to strong surface recombination in the depletion region, giving rise to an IV-behavior similar to that with low shunt resistance. Importantly, we find that the open-circuit voltage of nanowire solar cells is typically limited by contact leakage. Therefore, to increase the efficiency, we have investigated the effect of high-bandgap GaP carrier-selective contact segments at the top and bottom of the InP nanowire and we find that GaP contact segments improve the solar cell efficiency. Next, we discuss the merit of p-i-n and p-n junction concepts in nanowire solar cells. With GaP carrier selective top and bottom contact segments in the InP nanowire array, we find that a p-n junction design is superior to a p-i-n junction design. We predict a best efficiency of 25% for a surface recombination velocity of 4500 cm/s, corresponding to a non-radiative lifetime of 1 ns in p-n junction cells. The developed 1D model can be used for general modeling of axial p-n and p-i-n junctions in semiconductor nanowires. This includes also LED applications and we expect faster progress in device modeling using our method.

Keywords: Opto-electronic modeling, semiconductor nanowire, pn-junction, solar cell

1. Introduction

Photovoltaics, which transforms solar radiation directly into electrical power, has been realized for example in semiconductor planar and nanostructured solar cells [1-3]. Importantly, nanostructures, such as nanowire arrays (see inset in Figure 1a), can achieve absorption comparable to planar structures while using less material [4, 5]. Due to this broadband absorption at lower material consumption, nanowire arrays have attracted attention for solar cell applications in both experimental [1, 6-8] and theoretical studies [4, 9-16].

InP and GaAs are promising materials for nanowire array solar cells thanks to their respective band gap, which is well matched for absorption of the solar spectrum [1, 7, 17]. For GaAs nanowires, surface passivation is important because of the high surface recombination velocity of GaAs and large surface to volume ratio of nanowires [1]. An efficiency of 15.3% has been reached in an epitaxially fabricated GaAs nanowire array solar cell after passivating the nanowires with an AlGaAs shell [1]. For InP nanowires, efficiencies of 13.8% [7] and 17.8% [17] have been reached without intentional surface passivation in epitaxially fabricated arrays and top-down fabricated arrays, respectively. In this study, we focus on InP nanowire array solar cells, but we expect the main results and guidelines to apply also to well-passivated GaAs nanowires.

For InP nanowire array solar cell, previous experimental studies have demonstrated impressive short-circuit currents [1, 7, 17] with a highest reported value of 29.3 mA/cm^2 for an InP nanowire array solar cell [17]. However, the short-circuit current density (J_{sc}) is extracted at zero voltage where the efficiency is zero. Here, we optimize through modeling the full IV-curve of an InP nanowire solar cell to maximize the output power and hence the efficiency.

The nanowire array is an inherently three-dimensional (3D) structure, and computationally heavy 3D opto-electronics modeling is usually performed for theoretical studies of nanowire solar cells [13, 16]. We demonstrate an accurate 1D modeling method for nanowire arrays by (i) transforming the 3D photogeneration profile into an axially dependent 1D profile and (ii) transforming the surface recombination into an effective bulk recombination to allow 1D electrical modeling. The 1D modeling is orders of magnitude faster than 3D modeling and works for both strong and weak surface recombination. Furthermore, thanks to the 1D description, we can analyze the nanowire IV-curve using well-known textbook concepts

pertaining to planar pn-junctions. Such intuitive analysis allows for efficient design of nanowire devices with axial p-n and p-i-n junctions, also beyond solar cell applications.

First, we show how the superposition principle of $J(V)=J_{sc}-J_{dark}(V)$, with J_{dark} the current through the cell in the dark without incident light, can break down in nanowires when a high surface recombination velocity causes a noticeable recombination in the depletion region. Such a breakdown of the superposition principle shows up in the IV-curve in a similar fashion as a low shunt resistance and could have direct effect when assessing losses in experimentally measured IV-curves.

Next, we analyze the ideality factor of the nanowire IV-curve for varying surface recombination velocity. We found that for high surface recombination velocity, surface recombination in the depletion region causes an ideality factor of 2 and limits the open-circuit voltage (V_{oc}) and fill factor (FF); and hence the efficiency. For low surface recombination velocity, we find at a higher voltage an ideality factor of 1, which is shown to be set by leakage of minority carriers to the contacts. Thus, in a well-passivated nanowire, contact leakage limits the efficiency. Therefore, we propose the use of a high bandgap GaP segment at the top and at the bottom of the nanowire to block minority carriers from leaking to the contacts. With such GaP segments, we can reach a V_{oc} close to that in the radiatively limited Shockley-Queisser detailed balance analysis and an efficiency of 29.6%.

Finally, we turn to question the commonly used p-i-n junction design in nanowires, which is used to create an electric drift field in the long intrinsic region. Such a drift field separates effectively the photogenerated carriers in the intrinsic region and blocks those photogenerated minority carriers from reaching the contacts where they could recombine leading to a lowering of J_{sc}. However, a long intrinsic region opens at the same time up for additional V_{oc}-limiting recombination. With the GaP selective contacts, we can actually rely on diffusion to separate the carriers if the non-radiative lifetime is long enough. We can then, to enhance V_{oc}, move from the p-i-n to a p-n junction design that has a much shorter depletion region. With such a design, we can reach an efficiency of 25% even for a surface recombination velocity of 4500 cm/s, corresponding to a non-radiative lifetime of 1 ns, showing that considerable headroom exists compared to the current experimental record efficiency of 17.8% [17].

2. Methods

Unless otherwise stated, we consider a square lattice p-i-n InP nanowire array with 330 nm period. The nanowires have a radius of 90 nm and a length of 1400 nm (see inset in Figure 1a), which give a high short circuit current [18]. The doping level in both the top n and bottom p segment is 10^{18} cm^{-3} with a length of 100 nm for the n segment and 300 nm for the p segment. The substrate is 300 nm thick and of p-type with the same doping level as in the p segment of the nanowire. On top of the n segment and at the bottom of the substrate, we place ideal Ohmic contacts [18].

We perform full opto-electronic modeling of the nanowire-array solar cell with the finite element method in Comsol, which includes drift-diffusion modeling for the electron and hole transport and optics modeling for the absorption of light and the photogeneration of electron-hole pairs (see Ref. [18] for details and materials parameters used). From the optics modeling with the Maxwell equations, we obtain the 3D optical generation rate

$$g_{3D}(\mathbf{r}) = \int_{280\text{nm}}^{\lambda_{\text{bandgap}}} \frac{A_e(\mathbf{r},\lambda)}{E_{\text{photon}}} d\lambda \quad (1)$$

where A_e is the absorbed energy density at position $\mathbf{r}$ in the nanowire for incident light with wavelength λ and E_{photon} is the corresponding photon energy. We use in the calculation the AM1.5D solar spectrum, which shows negligible intensity at wavelength below 280 nm. For the 1D drift-diffusion modeling, we average the photogeneration rate in the cross-section of the nanowire of radius r_{NW}:

$$g_{1D}(z) = \frac{\int_0^{2\pi}\int_0^{r_{NW}} g_{3D}(r,\theta,z) dr d\theta}{\pi {r_{NW}}^2}. \quad (2)$$

See Supporting Information Figure S1 for the validity of using g_{1D} instead of g_{3D} in 3D modeling. Note that g_{1D} can be obtained for many cases also from the scattering matrix method, which can be computationally orders of magnitude faster than the finite element method (see Supporting Information Figure S2). Full opto-electrical modeling of a nanowire array with nanowires of a length of 1400 nm took us 36 core hours on a dual 16-core DELL Precision Tower 7910 in 3D modeling but only 5 core minutes when combining the 1D electrical modeling described below with the scattering matrix method for calculating g_{1D}.

In our electrical modeling, we assume that the surface recombination is of Shockley-Read-Hall (SRH) type and given by [18]

$$R_{\mathrm{surface}} = \frac{v_{\mathrm{sr}}}{n+p+2n_{\mathrm{i}}}(np - {n_{\mathrm{i}}}^2) \quad (3)$$

at the surface of the nanowire, with v_{sr} the surface recombination velocity, $n(\mathbf{r})$ the electron concentration, $p(\mathbf{r})$ the hole concentration, and n_i the intrinsic carrier concentration in the semiconductor. Also for non-radiative bulk recombination, we assume a SRH type recombination of $R_{bulk} = A_{bulk}(np-n_i^2)/(n+p+2n_i)$ (with $A_{bulk} = 10^7$ s^{-1} unless otherwise stated [18]). Thus, the surface and bulk SRH recombination is of similar form, with the only difference being where they are defined (the surface of circumference $2\pi r_{NW}$ or the full cross-section of area πr_{NW}^2). Now, we can translate the surface recombination into an additional, effective bulk recombination term, with recombination parameter A_{eff}, giving:

$$\int_0^{2\pi} \frac{v_{\mathrm{sr}}(z)[n(r_{\mathrm{NW}},\theta,z)p(r_{\mathrm{NW}},\theta,z)-{n_i}^2]r_{\mathrm{NW}}d\theta}{n(r_{\mathrm{NW}},\theta,z)+p(r_{\mathrm{NW}},\theta,z)+2n_{\mathrm{i}}} = \int_0^{2\pi}\int_0^{r_{\mathrm{NW}}} \frac{A_{\mathrm{eff}}(z)[n(r,\theta,z)p(r,\theta,z)-{n_{\mathrm{i}}}^2]rdrd\theta}{n(r,\theta,z)+p(r,\theta,z)+2n_{\mathrm{i}}} \quad (4)$$

From Eq. (4), we can solve for A_{eff} and perform 1D electrical modeling with (A_{eff}+A_{bulk}) as the recombination parameter where A_{bulk} is the original bulk recombination parameter. Note that we allow here in principle for an axially varying v_{sr} through the z-dependence in Eq. (4).

At low v_{sr}, n and p show negligible variation over the cross-section of the nanowire, and we obtain, from Eq. (4), $2\pi r_{NW}v_{sr} = \pi r_{NW}^2 A_{eff}$, which gives, similarly as in Ref. [19]:

$$A_{eff} = 2v_{sr}/r_{NW} \quad (5)$$

With increasing v_{sr}, the surface recombination causes a lower carrier density at the circumference of the cross-section, where the recombination occurs, compared to at the center of the cross-section. In that case, the assumption of constant carrier concentration within the cross-section of the nanowire, which gives the above $A_{eff} = 2v_{sr}/r_{NW}$, over-estimates the surface recombination (explaining why in Figure 1 the J_{sc} and V_{oc} are lower, due to over-estimated recombination, in the 1D modeling when using Eq. (5) for the highest $v_{sr} = 10^6$ cm/s as compared to with full 3D modeling).

We can correct for this over-estimation of recombination at high v_{sr} by adjusting A_{eff}. We calculated the current in 3D modeling and modified the A_{eff} according to these results. Based

on the solutions of drift diffusion equations (see Figure 1 (a)), we found the following equation for A_{eff} to yield good agreement between our 1D and 3D modeling:

$$A_{\text{eff}} = A_0 \frac{2v_{\text{sr}}}{r_{\text{NW}}} \tag{6}$$

where

$$A_0 = \min[\tfrac{1}{4}\log_{10}\left(\frac{v_0}{v_{\text{sr}}}\right), 1] \tag{7}$$

with v_0 a term that depends on the mobility/diffusion of electrons and holes and the nanowire radius. For InP nanowires of 90 nm in radius and $\mu = \mu_{\text{InP}}$ = 5400 (200) $\text{cm}^2\text{V}^{-1}\text{s}^{-1}$ in mobility for electrons (holes), we suggest the value $v_{0,\text{InP}} = 10^7$ m/s for v_0. When varying the radius and mobility, we found (see Supporting Information Figure S3) that the parameter v_0 was given by:

$$v_0 = (\frac{r_{\text{NW}}}{r_0})^{-\log_2(10)} \alpha v_{0,\text{InP}} \tag{8}$$

where r_0 is 90 nm and $\mu = \alpha\mu_{\text{InP}}$ for both electrons and holes.

3. Results

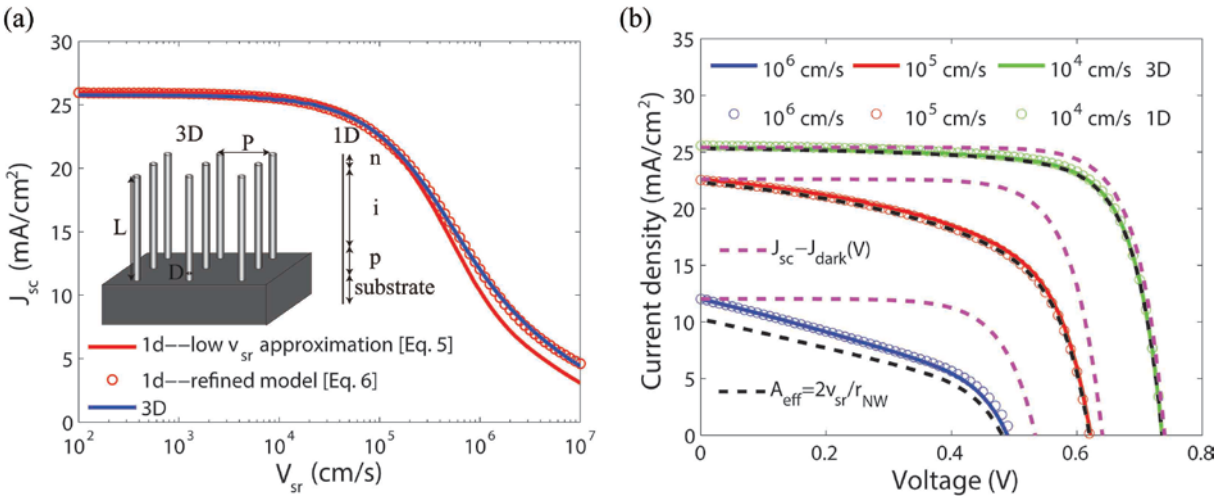

Figure 1. (a) Short circuit current density as a function of surface recombination velocity in both 3D and 1D model. (b) Current voltage response of nanowire array solar cells with different surface recombination velocity as marked in the figure (3D modeling with solid lines, 1D modeling with low-v_{sr} approximation from Eq. (5) with dashed black lines, 1D modeling with refined model for surface recombination from Eq. (6) with circles), together with J_{sc} - J_{dark}(V) from the superposition principle with 3D modeling (dashed magenta lines).

We turn to verify the above 1D modeling scheme by comparing the results with those from full 3D modeling that uses the 3D photogeneration profile $g_{3\text{D}}(\mathbf{r})$ and takes into account

surface recombination with v_{sr} at the surface of the nanowire through Eq. (3). First, we consider the J_{sc}, which is defined at zero voltage bias (Figure 1a). From the 3D modeling, we find that the J_{sc} starts to decrease noticeably for $v_{sr} > 10^4$ cm/s, and for $v_{sr} = 10^7$ cm/s, the J_{sc} has dropped by 80%, in agreement with previous studies [13, 14].

When we perform 1D modeling of J_{sc} with $g_{1D}(z)$ from Eq. (2) and A_{eff} from Eq. (5), which assumes a low v_{sr} to take into account the surface recombination, we find good agreement between 1D and full 3D modeling for $v_{sr} < 10^5$ cm/s (Figure 1a). However, for increasing v_{sr}, the results between 1D and 3D modeling deviate. For the highest considered v_{sr} of 10^7 cm/s, the discrepancy is 1.3 mA/cm^2, which corresponds to 30% of the short-circuit current density. This deviation can be decreased by using in the 1D modeling the A_{eff} from Eq. (6), which applies also at large v_{sr}. With that refined A_{eff}, the short circuit current agrees much better between 3D and 1D model at high v_{sr}, with a discrepancy below 0.2 mA/cm^2 at $v_{sr} =10^7$ cm/s.

Next, we turn to study the full IV-curve of the solar cell (Figure 1b) at $v_{sr} = 10^4$, 10^5, and 10^6 cm/s for which the J_{sc} varied noticeably in Figure 1a. We find that the low v_{sr} assumption of $A_{eff} = 2v_{sr}/r_{NW}$ [Eq. (5)] in the 1D model works well for $v_{sr} = 10^4$ and 10^5 cm/s. However, for $v_{sr} = 10^6$ cm/s, we find much better agreement between the 1D and 3D modeling when we use the refined A_{eff} from Eq. (6) with maximum difference of about 0.01 V in V_{oc} and 0.01 in FF, with FF defined as $P_{max}/(J_{sc}V_{oc})$ where P_{max} is the maximum output power.

Thus, the simple, low v_{sr} approximation of $A_{eff} = 2v_{sr}/r_{NW}$ from Eq. (5) works here for the modeling up to $v_{sr} = 10^5$ cm/s, which covers the range where we expect efficient nanowire solar cells. For higher v_{sr}, we can use the refined, but more complicated, A_{eff} from Eq. (6) to analyze the IV-behavior of nanowire solar cells.

Importantly for nanowire solar cell characterization, in Figure 1b, we see that for v_{sr} of 10^5 and 10^6 cm/s, the IV curve slopes noticeably already at $V = 0$, which typically indicates the presence of a shunt resistor parallel to the junction [20]. However, in our modeling, no such shunt resistor is present. Instead, our 1D analysis reveals (Figure 1b) that we are observing for $v_{sr} > 10^4$ cm/s increasing breakdown of the superposition principle, in which we assume that the IV-curve under illumination, $J(V)$, is given by $J_{sc} - J_{dark}(V)$. The failure of the superposition principle is caused by the change in carrier concentrations in the intrinsic region at low voltage between dark and illuminated conditions (see Figure S4 and S5), similarly as reported for the depletion region in a p-n junction Si cell [21]. Therefore, a sufficiently strong

recombination mechanism, through a high v_{sr}, increases the recombination rate in the illuminated case compared to in the dark case, which breaks down the superposition principle. In contrast, in nanowires with low v_{sr}, the superposition principle holds well, even at low voltage, despite the change in carrier concentrations between dark and illuminated conditions.

Previously, optics modeling and full opto-electronic modeling has recommended to increase the nanowire length to enhance the short-circuit current of the nanowire solar cell [9, 10]. Here, we study the effect of increasing nanowire length on the full IV-curve of the solar cell, by making the intrinsic segment longer, starting from the 1400 nm long nanowires. For low surface recombination velocity, the efficiency shows a maximum for a nanowire length of approximately 2 μm with the highest value of 22.4% (Figure 2a). For v_{sr} of 10^4 cm/s or higher, the efficiency decreases monotonously when the nanowire length is increased. Thus, here we find that, irrespective of the v_{sr}, the nanowire length cannot be increased without limit in an attempt to increase efficiency.

To understand this limitation on nanowire length, first the short circuit current is studied in Figure 2b. At zero surface recombination velocity, short circuit current increases monotonously with length. The current rises up to a fixed value of 27.6 mA/cm^2, which is limited by the reflection loss at the top of the nanowire array and the less than 100% extraction of photogenerated carriers from the top n-region [18]. A minor decrease is found beyond 9 μm in length for $v_{sr} = 10^2$ cm/s, indicating that surface recombination in the intrinsic region starts to limit J_{sc}. For $v_{sr} = 10^4$ cm/s, the surface recombination limits strongly the J_{sc}. At the highest considered v_{sr} of 10^6 cm/s, a rapid decrease in short circuit current can be seen with increasing nanowire length in Figure 2b, which leads to a similar rapid drop in the solar cell efficiency. Thus, the rapid drop in J_{sc} with increasing nanowire length is the main limiting factor for efficiency for nanowires with high surface recombination velocity.

Next, open circuit voltage as a function of nanowire length is studied in Figure 2c. For the case of zero surface recombination, V_{oc} is limited to approximately 0.9 V for short wires. For all v_{sr}, open circuit voltage decreases with increasing nanowire length as a longer intrinsic region increases the possibility of recombination. For 10 μm long nanowires, even a very low surface recombination velocity of 10^2 cm/s leads to a decrease of 0.06 V in open circuit voltage compared to in 1.4 μm long nanowires. For high surface recombination velocity of 10^4 and 10^6 cm/s, the open circuit voltage appears to decrease linearly with a ratio of about 0.04 V/μm.

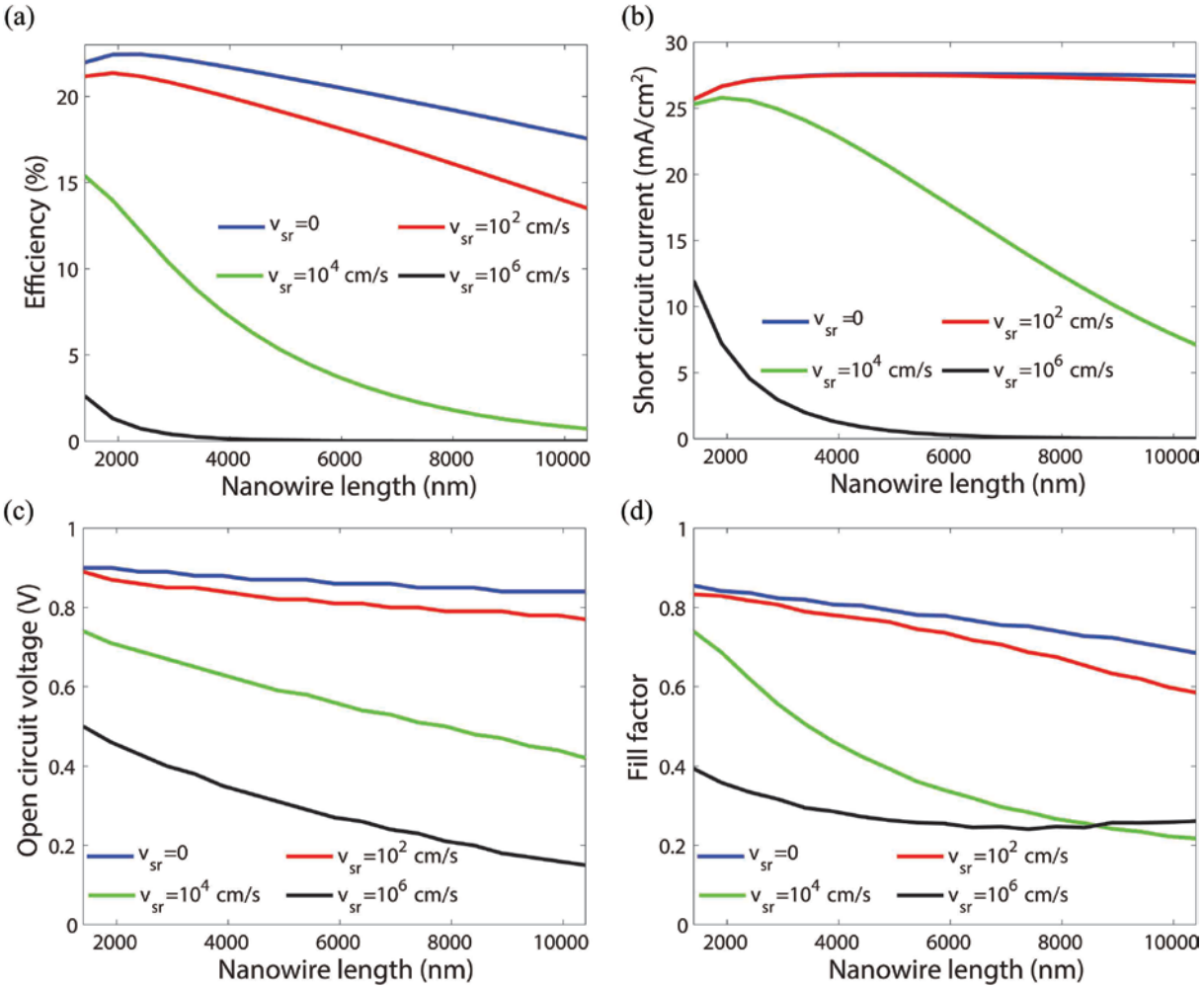

Figure 2. Efficiency (a), short circuit current (b), open circuit voltage (c) and fill factor (d) as a function of InP nanowire length for different surface recombination velocity with fixed length of n and p segment and varying length for i segment.

Finally, an increase of the nanowire length is harmful also to the fill factor for all values of v_{sr} (Figure 2d). Importantly, for low v_{sr} of 0 and 100 cm/s, the fill factor of 10 µm long nanowires drops by 20% compared to that in 1400 nm long nanowires. Thus, the decrease in fill-factor with increasing nanowire length is the main efficiency limiting factor in nanowires showing low surface recombination velocity.

To go beyond this efficiency of 22.4% that was found for v_{sr} = 0 (Figure 2a), we note that the V_{oc} was limited to 0.9 V (Figure 2c) considerably below the Shockley-Queisser limit of 1.02 V, which is the limit set by radiative recombination [22]. To reveal the recombination mechanisms limiting V_{oc}, we perform a study of the voltage dependent ideality factor $n_{ideality} = q(dJ_{dark}/dV)^{-1}J_{dark}/k_BT$ where k_B is the Boltzmann constant and T = 300 K the temperature in our modeling [23] (see Figure 3). As a note, the ideality factor is 2 when surface or bulk SRH

recombination in a depletion region dominates, 1 when surface or bulk SRH recombination in a doping region dominates, 1 when radiative recombination dominates, and 1 when contact leakage, that is, leakage of minority carriers to the contact, dominates [24].

First, for all v_{sr} considered, at high voltage, and consecutively at high current density, resistive losses within the nanowire come into play leading to an ideality factor above 2. Second, for low voltages, we find for all v_{sr} an ideality factor of 2 due to surface and/or bulk SRH recombination in the i-segment. Third, for $v_{sr} = 10^4$ cm/s, an ideality factor between 1 and 2 shows up [24], and at a voltage of about 1 volt, a bump shows up in the ideality factor due to competition between surface recombination in the different regions (depleted intrinsic region vs. n and p doping regions). Fourth, when we consider the case of $v_{sr} = 0$, we find an ideality factor close to 1 between 0.8 and 1.1 V. A detailed analysis shows that this ideality factor of 1 is set by contact leakage. Thus, contact leakage is a major barrier towards a high efficiency InP nanowire array solar cell with above 0.9 V in V_{oc}.

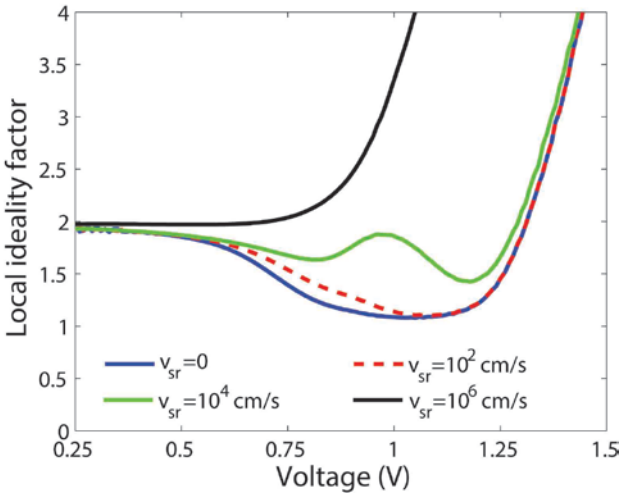

Figure 3. Voltage dependent local ideality factor of InP nanowire array p-i-n junction.

In our previous study, a 100 nm long GaP segment was used on top of the InP n-segment as a selective contact. The high-bandgap GaP segment shifts a major part of the photogeneration to the underlying InP segment and blocks photogenerated minority carriers from diffusing to the top contact from the intrinsic region, leading to a boost in J_{sc} with an almost 100% internal quantum efficiency for the collection of optical generated carriers [18]. However, such a GaP top segment does not increase noticeably the V_{oc} of the InP nanowire solar cell (compare blue curve and dashed red curve in Figure 4a). At forward bias, high mobility electrons are injected into the bottom p-segment, and they can diffuse to the bottom contact and recombine, limiting the V_{oc}.

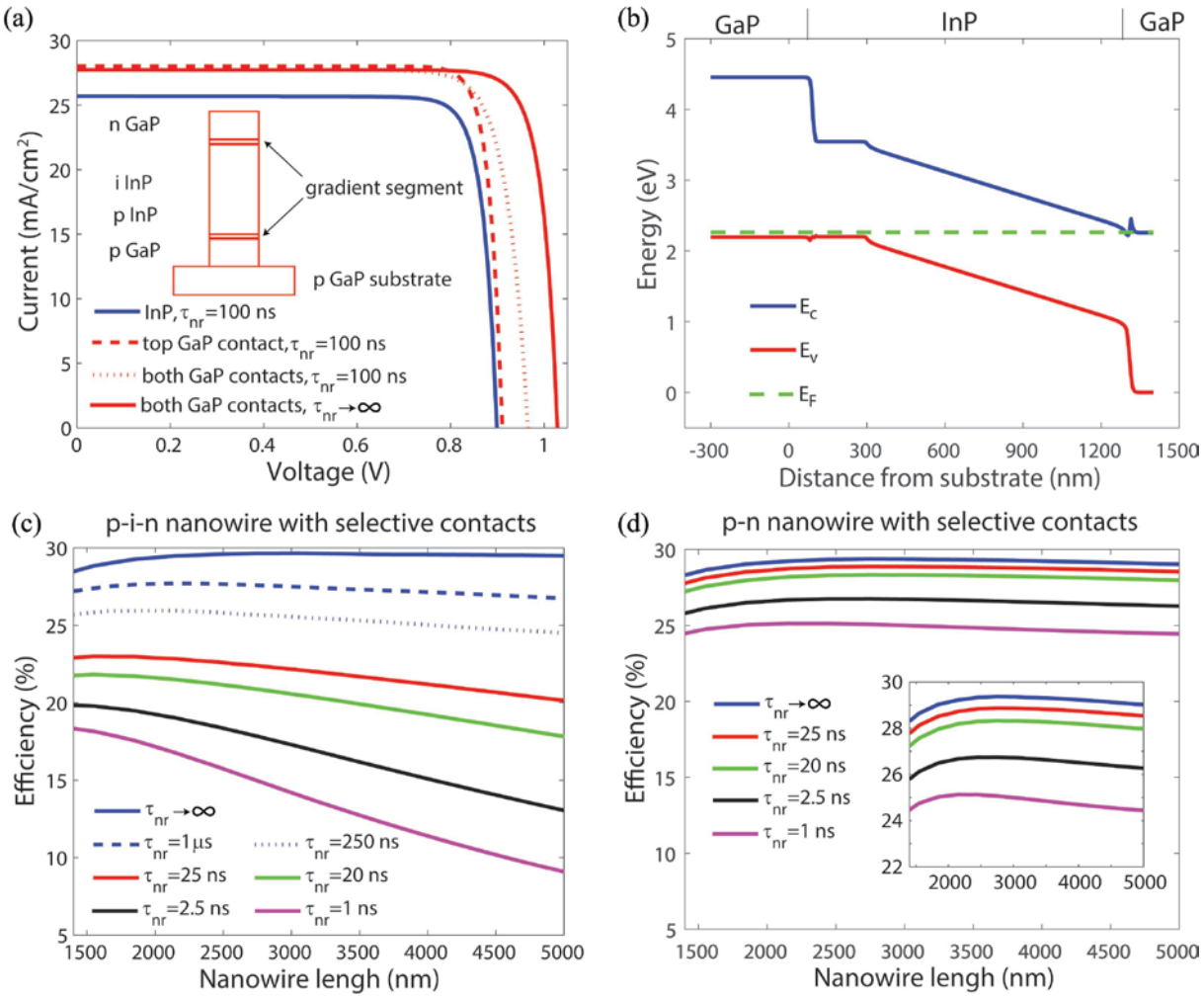

Figure 4. (a) Current voltage response of InP nanowire array with and without GaP selective contact(s)/segment(s). A 20 nm long, linearly graded $Ga_xIn_{x-1}P$ segment is placed between GaP and InP segments. For the material parameters of $Ga_xIn_{x-1}P$, we use linear interpolation between those of InP and GaP. (b) Band diagram with valence band E_v, conduction band E_c, and Fermi energy E_F of InP nanowire array with top and bottom GaP selective contacts at zero voltage in the dark. Parameters of GaP and InP can be found in Ref. [18]. (c, d) Nanowire array solar cell efficiency as a function of nanowire length for different non-radiative lifetime τ_{nr}. The inset figure shows the peak positions. The length is 100 nm for both the top n and bottom p GaP segment. In (c), the length of the p InP segment is fixed to 200 nm and the length of the intrinsic segment varies. In (d), the intrinsic InP segment is replaced by p InP and the inset is a zoom-in that shows the maxima clearer.

Therefore, we include here additionally a p type GaP bottom segment with the nanowires on a GaP substrate to block the diffusion of electrons to the bottom contact at forward bias (solid red line in Figure 4a – see Figure 4b for the band diagram with top and bottom GaP selective contacts; at the GaP/InP interfaces, minority carriers are reflected by the GaP barrier and the contact recombination is reduced significantly). The open circuit voltage increases to 0.97 V for a non-radiative lifetime of τ_{nr} = 100 ns, corresponding to v_{sr} = 0 and $A_{bulk} = 10^7$ s^{-1} (dotted red line in Figure 4a). Here, we define $\tau_{nr} \equiv 1/(A_{eff} + A_{SRH})$ (note that thanks to our 1D analysis,

we don't need to consider surface and bulk SRH recombination separately; and Auger recombination is in our systems small enough to be ignored for the non-radiative lifetime [18]). For $\tau_{nr} \rightarrow \infty$, this design with selective top and bottom contact can improve the open circuit voltage to 1.02 V, which is close to the Shockley-Queisser radiative limit (note that throughout our modeling, we used the bulk *B* parameter for radiative recombination in InP; see Supporting Information of Ref. [18]). Thus, with the GaP carrier-selective segments, the performance of the nanowire cell is not limited by contact leakage any longer but by the surface and lattice quality.

In Figure 4c, the efficiency as a function of nanowire array length is shown for varying non-radiative lifetime τ_{nr}. For zero non-radiative recombination, that is, for $\tau_{nr} \rightarrow \infty$, an efficiency of 29.6% is found. A long non-radiative lifetime of 1 μs drops the maximum efficiency to 27.7%, which is found for 2 μm long nanowires. For τ_{nr} = 250 ns, the maximum efficiency reduces to 26%. The lowest reported value for the surface recombination velocity in InP nanowires is 170 cm/s [25], which corresponds to τ_{nr} = 25 ns from the A_{eff} in Eq. (5). Such a lifetime reduces the best efficiency to 23%, which is found with 2 μm long nanowires. For τ_{nr} = 1 ns, we find a maximum efficiency of 18.3 %.

In the above p-i-n nanowire designs, the drift field is used to enhance J_{sc}. For strong non-radiative recombination, diffusion lengths can become too short for efficient diffusion-driven separation of photogenerated carriers. On the other hand, for weak non-radiative recombination, diffusion of photogenerated minority carriers to the contacts can lead to noticeable contact leakage and loss in J_{sc}. A drift field can enhance the separation of photogenerated carriers and limit contact leakage, giving an almost 100% internal quantum efficiency in the i-segment [18]. However, a long intrinsic segment tends to be counterproductive for V_{oc} by opening up for more recombination at forward bias.

When we include the carrier selective n and p GaP segments at the top and the bottom of the nanowire to limit contact leakage, we could rely on diffusion for charge separation if the non-radiative recombination is weak. Thus, the long intrinsic region with a drift field might not be needed. We demonstrate in Figure 4d results for a nanowire where the intrinsic region is replace by a p-doped segment. Indeed, for all values of τ_{nr} considered, the efficiency is enhanced in this p-n junction design over that in the p-i-n junction design shown in Figure 4c. For example, it is possible to reach a high efficiency of 25% with τ_{nr} = 1 ns, which corresponds to a surface recombination velocity of 4500 cm/s (in comparison, to reach an

efficiency of 25% with the p-i-n design, τ_{nr} > 100 ns is needed). Note that when we include effects from a lower mobility in the p-doped segment than in the intrinsic segment, the highest efficiency values drop by approximately 1%, but the p-n junction still gives higher efficiency than the p-i-n junction (see Supporting Information Figure S6).

4. Conclusions

We developed a 1D modeling method for axial p-n and p-i-n junction nanowire array solar cells. This 1D modeling is about 400 times faster than 3D modeling. With the intuitive 1D modeling, we could use concepts from planar solar cells to analyze and optimize the behavior of the nanowire-array solar cell. Most importantly, we showed that to enhance the performance of nanowire solar cells, it is beneficial to include high-bandgap top and bottom carrier-selective segments and move to a p-n junction design from the commonly used p-i-n junction design.

Acknowledgments

This work was performed within NanoLund and received funding from the People Programme (Marie Curie Actions) of the European Union's Seventh Framework Programme (FP7-People-2013-ITN) under the REA grant agreement no. 608153, PhD4Energy, and the European Union's Horizon 2020 research and innovation programme under grant agreement no. 641023, NanoTandem. This article reflects only the author's view and the funding agency is not responsible for any use that may be made of the information it contains. Kivisaari wants to express his gratitude to the Nokia Foundation, the Walter Ahlström Foundation and the Emil Aaltonen Foundation for financial support.

References

1. Åberg, I., et al., *A GaAs nanowire array solar cell with 15.3% efficiency at 1 sun.* IEEE Journal of Photovoltaics, 2016. **6**(1): p. 185-190.
2. Martin A. Green, K.E., Yoshihiro Hishikawa, Wilhelm Warta, Ewan D. Dunlop, Dean H. Levi and Anita W. Y. Ho-Baillie, *solar cell efficiency table (version 49).* Progress in Photovoltaics: Research and Applications, 2017. **25**: p. 3-13.
3. Otnes, G. and M.T. Borgström, *Towards high efficiency nanowire solar cells.* Nano Today, 2016. **12**: p.31-45.
4. Hu, L. and G. Chen, *Analysis of optical absorption in silicon nanowire arrays for photovoltaic applications.* Nano letters, 2007. **7**(11): p. 3249-3252.
5. Kelzenberg, M.D., et al., *Enhanced absorption and carrier collection in Si wire arrays for photovoltaic applications.* Nature materials, 2010. **9**(3): p. 239-244.
6. Mariani, G., et al., *Direct-Bandgap Epitaxial Core–Multishell Nanopillar Photovoltaics Featuring Subwavelength Optical Concentrators.* Nano letters, 2013. **13**(4): p. 1632-1637.

7. Wallentin, J., et al., *InP nanowire array solar cells achieving 13.8% efficiency by exceeding the ray optics limit.* Science, 2013. **339**(6123): p. 1057-1060.
8. Yao, M., et al., *Tandem solar cells using GaAs nanowires on Si: design, fabrication, and observation of voltage addition.* Nano letters, 2015. **15**(11): p. 7217-7224.
9. Anttu, N. and H. Xu, *Efficient light management in vertical nanowire arrays for photovoltaics.* Optics express, 2013. **21**(103): p. A558-A575.
10. Huang, N., C. Lin, and M.L. Povinelli, *Limiting efficiencies of tandem solar cells consisting of III-V nanowire arrays on silicon.* Journal of Applied Physics, 2012. **112**(6): p. 064321.
11. LaPierre, R., *Theoretical conversion efficiency of a two-junction III-V nanowire on Si solar cell.* Journal of Applied Physics, 2011. **110**(1): p. 014310.
12. Wang, B. and P.W. Leu, *Tunable and selective resonant absorption in vertical nanowires.* Optics letters, 2012. **37**(18): p. 3756-3758.
13. Wang, X., et al., *Performance-limiting factors for GaAs-based single nanowire photovoltaics.* Optics express, 2014. **22**(102): p. A344-A358.
14. Yu, S., F. Roemer, and B. Witzigmann, *Analysis of surface recombination in nanowire array solar cells.* Journal of Photonics for Energy, 2012. **2**(1): p. 028002-1-028002-9.
15. Huang, N. and M.L. Povinelli, *Design of passivation layers on axial junction GaAs nanowire solar cells.* IEEE Journal of Photovoltaics, 2014. **4**(6): p. 1511-1517.
16. Trojnar, A.H., et al., *Optimizations of GaAs Nanowire Solar Cells.* IEEE Journal of Photovoltaics, 2016. **6**(6): p. 1494-1501.
17. van Dam, D., et al., *High-Efficiency Nanowire Solar Cells with Omnidirectionally Enhanced Absorption Due to Self-Aligned Indium–Tin–Oxide Mie Scatterers.* ACS Nano, 2016. **10**(12): p. 11414-11419.
18. Chen, Y., et al., *Optimization of the short-circuit current in an InP nanowire array solar cell through opto-electronic modeling.* Nanotechnology, 2016. **27**(43): p. 435404.
19. Dan, Y., et al., *Dramatic reduction of surface recombination by in situ surface passivation of silicon nanowires.* Nano letters, 2011. **11**(6): p. 2527-2532.
20. Green, M.A., *Solar cells: operating principles, technology, and system applications.* 1982.
21. Robinson, S., A. Aberle, and M. Green, *Departures from the principle of superposition in silicon solar cells.* Journal of Applied Physics, 1994. **76**(12): p. 7920-7930.
22. Shockley, W. and H.J. Queisser, *Detailed balance limit of efficiency of p‐n junction solar cells.* Journal of applied physics, 1961. **32**(3): p. 510-519.
23. Zhu, D., et al., *The origin of the high diode-ideality factors in GaInN/GaN multiple quantum well light-emitting diodes.* Applied Physics Letters, 2009. **94**(8): p. 081113.
24. Sze, S.M., *Semiconductor devices: physics and technology*. 2008: John Wiley & Sons.
25. Joyce, H.J., et al., *Ultralow surface recombination velocity in InP nanowires probed by terahertz spectroscopy.* Nano letters, 2012. **12**(10): p. 5325-5330.